JACS
JOURNAL OF THE AMERICAN CHEMICAL SOCIETY
Article
pubs.acs.org/JACS

Intramolecular and Lateral Intermolecular Hole Transfer at the Sensitized TiO_2 Interface

Ke Hu,[†] Kiyoshi C. D. Robson,[‡] Evan E. Beauvilliers,[†] Eduardo Schott,[§] Ximena Zarate,[§] Ramiro Arratia-Perez,*[,∥] Curtis P. Berlinguette,*[,‡] and Gerald J. Meyer*[,†]

[†]Departments of Chemistry and Materials Science and Engineering, Johns Hopkins University, 3400 North Charles Street, Baltimore, Maryland 21218, United States

[‡]Department of Chemistry and Center for Advanced Solar Materials, University of Calgary, 2500 University Drive NW, Calgary, Alberta, Canada T2N-1N4

[§]Laboratorio de Bionanotecnología, Universidad Bernardo O'Higgins, General Gana 1780, Santiago, Chile

[∥]Departamento de Ciencias Químicas, Relativistic Molecular Physics Group, Universidad Andres Bello, Republica 275, Santiago, Chile

Supporting Information

ABSTRACT: Characterization of the redox properties of TiO_2 interfaces sensitized to visible light by a series of cyclometalated ruthenium polypyridyl compounds containing both a terpyridyl ligand with three carboxylic acid/carboxylate or methyl ester groups for surface binding and a tridentate cyclometalated ligand with a conjugated triarylamine (NAr_3) donor group is described. Spectroelectrochemical studies revealed non-Nernstian behavior with nonideality factors of 1.37 ± 0.08 for the $Ru^{III/II}$ couple and 1.15 ± 0.09 for the $NAr_3^{\bullet+/0}$ couple. Pulsed light excitation of the sensitized thin films resulted in rapid excited-state injection ($k_{inj} > 10^8\ s^{-1}$) and in some cases hole transfer to NAr_3 [$TiO_2(e^-)/Ru^{III}–NAr_3 \rightarrow TiO_2(e^-)/Ru^{II}–NAr_3^{\bullet+}$]. The rate constants for charge recombination [$TiO_2(e^-)/Ru^{III}–NAr_3 \rightarrow TiO_2/Ru^{II}–NAr_3$ or $TiO_2(e^-)/Ru^{II}–NAr_3^{\bullet+} \rightarrow TiO_2/Ru^{II}–NAr_3$] were insensitive to the identity of the cyclometalated compound, while the open-circuit photovoltage was significantly larger for the compound with the highest quantum yield for hole transfer, behavior attributed to a larger dipole moment change ($\Delta\mu$ = 7.7 D). Visible-light excitation under conditions where the Ru^{III} centers were oxidized resulted in injection into TiO_2 [$TiO_2/Ru^{III}–NAr_3 + h\nu \rightarrow TiO_2(e^-)/Ru^{III}–NAr_3^{\bullet+}$] followed by rapid back interfacial electron transfer to another oxidized compound that had not undergone excited-state injection [$TiO_2(e^-)/Ru^{III}–NAr_3 \rightarrow TiO_2/Ru^{II}–NAr_3$]. The net effect was the photogeneration of equal numbers of fully reduced and fully oxidized compounds. Lateral intermolecular hole hopping ($TiO_2/Ru^{II}–NAr_3 + TiO_2/Ru^{III}–NAr_3^{\bullet+} \rightarrow 2TiO_2/Ru^{III}–NAr_3$) was observed spectroscopically and was modeled by Monte Carlo simulations that revealed an effective hole hopping rate of $(130\ ns)^{-1}$.

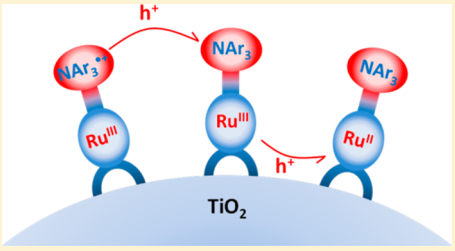

INTRODUCTION

Molecules with two or more redox-active groups have provided insights into interfacial electron transfer reactions at semiconductor interfaces that could not have been obtained from molecules with a single redox-active group.[1−8] A relatively common motif used for solar energy conversion in dye-sensitized solar cells is shown generically in Scheme 1. A sensitizing dye molecule S absorbs a photon to create an excited state that initiates two charge transfer reactions: (1) electron transfer to a TiO_2 nanocrystallite, and (2) intramolecular hole transfer to a covalently linked donor.[9] The net result is an interfacial charge-separated state comprising an injected electron and an oxidized donor. Here we report a study of 10 electron donor−acceptor compounds where the quantum yield for intramolecular hole transfer was systematically controlled.

Previous studies have shown that intramolecular hole transfer can lead to a dramatic enhancement of the lifetime of the electron that was injected into the semiconductor.[1,4] However, hole transfer comes at the expense of a significant loss in free energy for which the longer lifetime does not always compensate. It is therefore of interest to examine whether the driving force for hole transfer can be reduced without a loss in

Scheme 1. Excited-State Electron Injection and Intramolecular Hole Transfer for a Sensitizer−Linker−Donor Compound Anchored on a TiO_2 Surface.

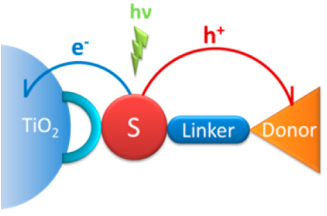

Received: October 18, 2013
Published: December 24, 2013

lifetime. Under such conditions, an "equilibrium" like that shown in Scheme 2 would be expected. This is not a true

Scheme 2. The Interfacial Redox Equilibrium under Study

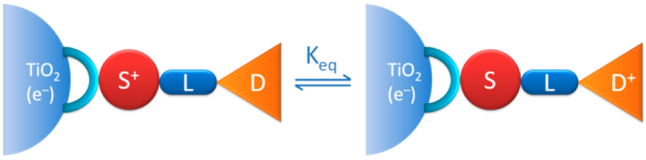

equilibrium, as recombination of the injected electron with the dye molecule is necessarily thermodynamically favored. Nevertheless, this recombination reaction is known to require milliseconds for completion[9] while intramolecular electron transfer occurs on a sub-nanosecond time scale,[2] so a quasi-equilibrium is expected on intermediate time scales and under steady-state illumination. Quantification of such a redox equilibrium is further complicated by the nonideal behavior of molecules anchored to conductive surfaces.[10,11] To our knowledge, with the one exception described below, no previous studies have characterized such interfacial equilibria and examined how they influence recombination or the free energy stored in the interfacial charge-separated state as reported by the open-circuit photovoltage.

In a recent communication,[8] electron transfer studies of three ruthenium terpyridyl compounds with a tridentate cyclometalated ligand conjugated to a triaryl amine donor located at TiO_2 interfaces were reported (Scheme 3). Light excitation of these sensitized materials led to rapid excited-state injection with hole transfer yields that could be qualitatively predicted on the basis of the solution reduction potentials. Surprisingly, the charge recombination rates were insensitive to the location of the oxidizing equivalent (i.e., Ru^{III} or $NAr_3^{\bullet+}$), while the open-circuit photovoltages were consistently larger for the compound that had undergone hole transfer. The coincidence of redox potentials and charge recombination kinetics suggested that the interfacial dipole moment contributed to the measured open-circuit photovoltage. Herein, DFT calculations have been employed to quantify the dipole moments before and after light excitation. A total of 10 donor–acceptor compounds with a broad range of $Ru^{III/II}$ and $NAr_3^{\bullet+/0}$ reduction potentials have been characterized so that the redox equilibrium in Scheme 3 could be systematically probed. In situ spectroelectrochemical results showed non-Nernstian behavior that provided new insights into the factors that control nonideality at semiconductor interfaces. In addition, a novel remote excited-state injection from a NAr_3 donor was observed under conditions where the ruthenium center was in the formal +III oxidation state. This excited-state injection was followed by rapid back electron transfer that was fast enough to compete with iodide oxidation. A lateral intermolecular hole hopping process was identified and modeled by Monte Carlo simulations.

EXPERIMENTAL SECTION

Materials. Acetonitrile (Burdick & Jackson, spectrophotometric grade), methanol (Sigma-Aldrich, spectrophotometric grade, >99.9%), *tert*-butanol (Fisher Scientific), lithium perchlorate (Aldrich, 99.99%), tetra-*n*-butylammonium hydroxide (TBAOH) (1 M in methanol, Sigma-Aldrich), argon gas (Airgas, >99.998%), oxygen gas (Airgas, industrial grade), titanium(IV) isopropoxide (Sigma-Aldrich, 97%), fluorine-doped SnO_2 (FTO)-coated glass (Hartford Glass Co., Inc., 2.3 mm thick, 15 Ω/sq), and glass microscope slides (Fisher Scientific, 1 mm thick) were used. The sensitizers in this study (**C1–C5** in Scheme 3) and their methyl ester derivatives (abbreviated similarly as **E1–E5**) were available from previous studies.[12]

Sensitized Metal Oxide Thin Films. Mesoporous nanocrystalline TiO_2 thin films were prepared as previously described.[13] The films were then immersed in **C1–C5** dye solutions in methanol with 1 equiv of TBAOH to help solubility or in **E1–E5** dye solutions in 50:50 (v/v) acetonitrile/*tert*-butanol. Films were then washed with neat CH_3CN and diagonally positioned in a standard 1 cm^2 quartz cuvette containing $LiClO_4$ solution (0.5 M in acetonitrile). The electrolyte solutions were purged with argon gas for at least 30 min prior to experimentation.

Spectroscopy. *UV–Vis Absorption.* Steady-state UV–vis absorption spectra were obtained on a Varian Cary 50 spectrophotometer. The experiments were performed at room temperature unless mentioned otherwise.

Transient Absorption Spectroscopy. Nanosecond transient absorption measurements were obtained with an apparatus similar to that previously described.[13] Samples were photoexcited by a frequency-doubled, Q-switched, pulsed Nd:YAG laser [Quantel USA (formerly Big Sky Laser Technologies) Brilliant B, 532 nm, 5–6 ns full width at half-maximum (fwhm), 1 Hz, ~10 mm in diameter] directed 45° to the film surface. A 150 W xenon arc lamp coupled to a 1/4 m monochromator (Spectral Energy Corp., GM 252) served as the probe beam (Applied Photophysics), which was aligned orthogonally to the excitation light. For detection at sub-100 μs time scales, the lamp was pulsed with 80 V. Detection was achieved with a monochromator

Scheme 3. Molecular Structures of the Compounds with the Indicated $Ru^{III/II}$ (blue) and $NAr_3^{\bullet+/0}$ (red) Reduction Potentials

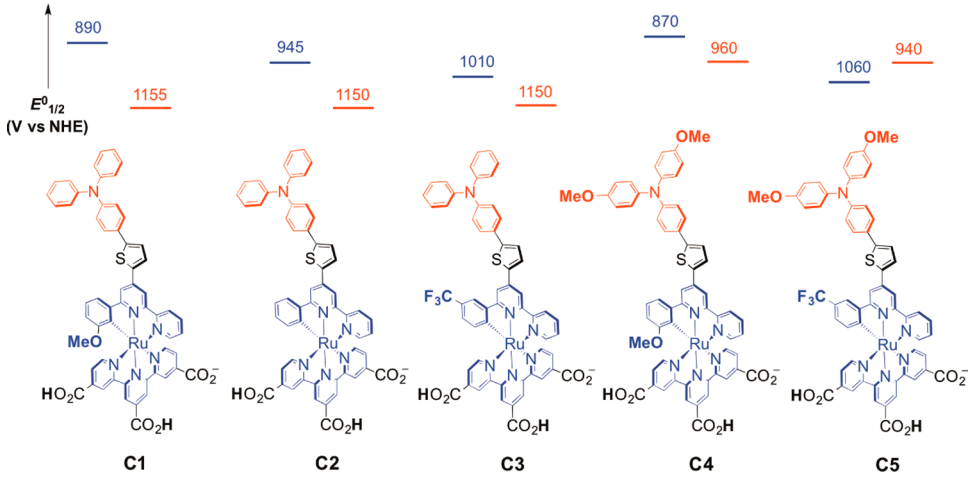

dx.doi.org/10.1021/ja410647c | J. Am. Chem. Soc. 2014, 136, 1034–1046

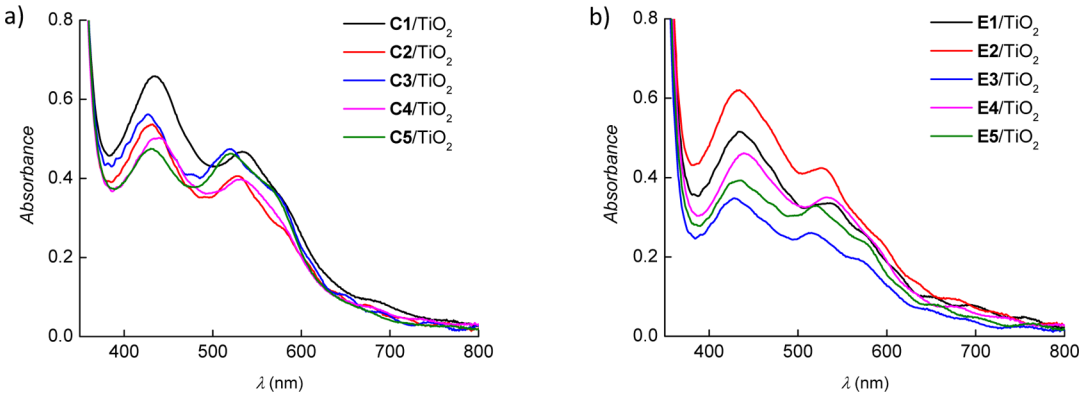

Figure 1. Visible absorption spectra of the indicated sensitized thin films immersed in 0.5 M $LiClO_4/CH_3CN$ solutions.

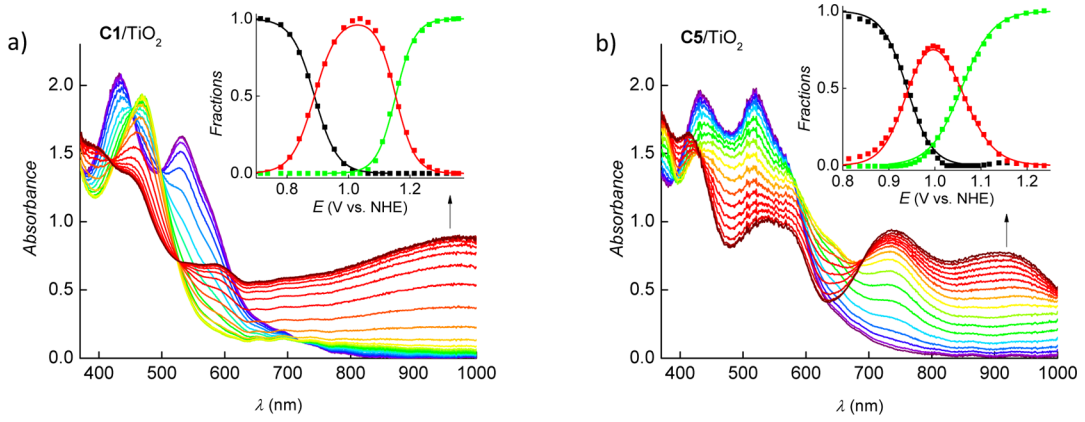

Figure 2. UV−vis−NIR absorption spectra of (a) **C1**/TiO_2 and (b) **C5**/TiO_2 measured at variable applied potentials in 0.5 M $LiClO_4/CH_3CN$ solutions. The arrows indicate the direction of absorption changes with increased positive applied potential. The insets show the fraction (x) of dye molecules present in the **C1**/TiO_2 or **C5**/TiO_2 (black solid squares), **C1**$^+$/TiO_2 or **C5**$^+$/TiO_2 (red solid squares), and **C1**$^{2+}$/TiO_2 or **C5**$^{2+}$/TiO_2 (green solid squares) states. Overlaid on the data are fits to a modified Nernst equation.

(Spex 1702/04) optically coupled to an R928 photomultiplier tube (Hamamatsu). Transient data were acquired on a computer-interfaced digital oscilloscope (LeCroy 9450, dual 350 MHz). Typically 30−50 laser pulses were averaged at each observation wavelength over the range 380−800 nm for full spectrum generation, and 120−200 laser pulses were averaged for single-wavelength measurements. For the low-temperature studies (−45 °C), the sample temperature was maintained to ±0.1 °C using a liquid nitrogen cryostat (UniSoku CoolSpek USP-203-B).

Infrared Absorption Spectroscopy. Attenuated total reflectance (ATR) spectra were obtained using a Thermo Scientific Nicolet Nexus 670 spectrophotometer. The measurements were made under a flow of N_2 gas, and the spectra were averaged over 128 scans with 1 cm^{-1} resolution.

Electrochemistry. A potentiostat (BAS model CV-50W) was employed for measurements in a standard three-electrode arrangement with a sensitized TiO_2 thin film deposited on an FTO substrate working electrode, a platinum disk counter electrode, and a Ag/AgCl reference electrode (Bioanalytical Scientific Instruments, Inc.) in acetonitrile containing 0.5 M $LiClO_4$. All potentials are reported versus the normal hydrogen electrode (NHE). The ferrocenium/ferrocene (Fc^+/Fc) half-wave potential was measured at room temperature before and after each experiment and was used as an external standard to calibrate the reference electrode. A conversion constant of −630 mV from NHE to Fc^+/Fc was used in acetonitrile at 25 °C.[14]

Spectroelectrochemistry. Steady-state UV−vis absorption spectra were recorded in concomitant with bulk electrolysis of a standard three-electrode cell. External biases were applied to the sensitized TiO_2 thin film deposited on an FTO substrate working electrode positioned diagonally in a 1 cm cuvette. Each potential step was held for around 2 to 3 min until the spectrum was invariant with time and the next potential was applied.

Computations. *Data Analysis.* Kinetic data fitting was performed in Origin 8.5, and least-squares error minimization was accomplished using the Levenberg−Marquardt iteration method. For the transient absorption spectral modeling and spectroelectrochemical determination of concentrations of redox-active states, a method for the standard addition of known spectra, written in Wolfram Mathematica 8.0, was implemented to realize least-squares error minimization.

Intermolecular Hole Hopping Kinetics Simulation. Monte Carlo simulations to model the lateral hole hopping process for **C1**$^+$/TiO_2 at variable laser fluences were performed with Wolfram Mathematica 8.0 and 9.0 on a personal computer (PC). Monte Carlo runs were repeated 1000 times for a single TiO_2 particle simulation (S/N ≥ 1000) while 50 runs were implemented for TiO_2 particle arrays (S/N ≥ 1350). The TiO_2 particle arrays were set to be 2 × 2 × 2 or 3 × 3 × 3, as larger arrays could not be minimized in a reasonable time period with a PC equipped with 16 GB of RAM.

DFT Calculations. The geometry optimizations and properties calculations of the ground-state and oxidized complexes were performed using the ADF2010.01 code.[15] The calculations were carried out using the ZORA Hamiltonian incorporating scalar (sc.) relativistic corrections[16−18] and the triple-ζ Slater basis set plus one polarization function (STO-TZP).[19,20] The molecular structures were fully optimized without symmetry constriction via analytical energy gradient techniques as implemented by Versluis and Ziegler,[21] employing nonlocal correction of exchange and correlation (XC) incorporated via the general gradient approximation (GGA) within the BP86 functional, which is composed of the exchange functional of Becke[22] and the correlation functional of Perdew.[23] Solvation effects

dx.doi.org/10.1021/ja410647c | J. Am. Chem. Soc. 2014, 136, 1034−1046

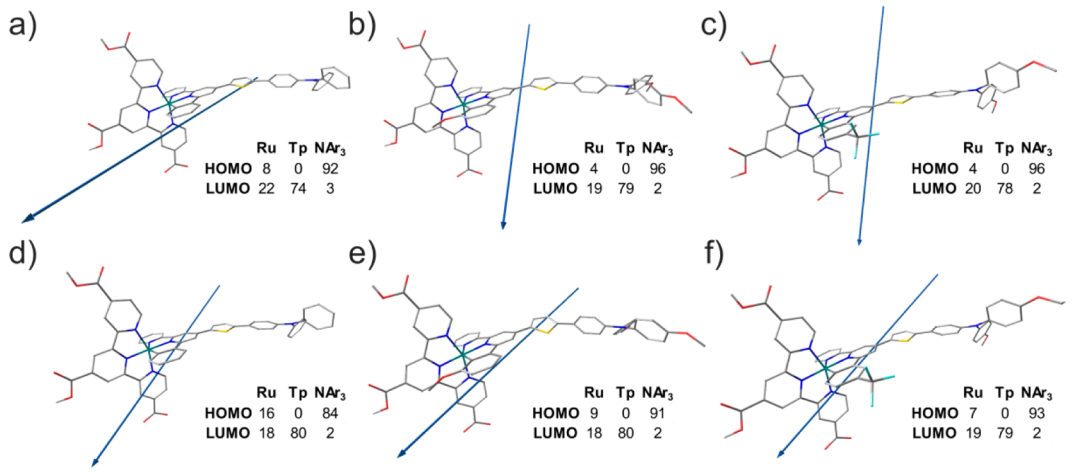

Figure 3. Calculated dipole moment vectors for (a) **C2**, (b) **C4**, (c) **C5**, (d) **C2**$^+$, (e) **C4**$^+$, and (f) **C5**$^+$. The table in each image shows the percentage contributions of ruthenium (Ru), the terpyridine (Tp), and the triarylamine (NAr_3) to the HOMO and LUMO.

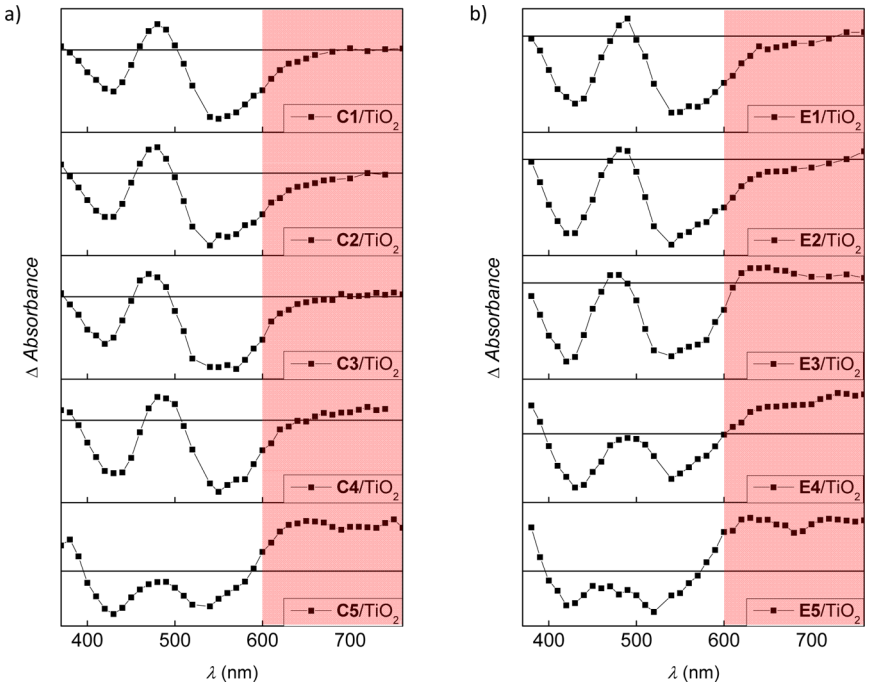

Figure 4. Absorption difference spectra measured at 100 ns delay time after pulsed 532 nm excitation of (a) **C1**/TiO_2–**C5**/TiO_2 and (b) **E1**/TiO_2–**E5**/TiO_2 immersed in 0.5 M $LiClO_4/CH_3CN$ solution. Regions highlighted in pink are where $NAr_3^{\bullet+}$ absorbs light strongly.

were modeled by the conductor-like screening model for real solvents (COSMO)[24,25] using acetonitrile as the solvent for all of the calculations.

RESULTS

The carboxylic forms of the compounds anchored to mesoporous anatase TiO_2 thin films with high surface coverages ($>3 \times 10^{-8}$ mol/cm^2) within reaction times of 1 h in methanol solutions at room temperature. The ground-state absorption of these sensitized thin films immersed in 0.5 M $LiClO_4/CH_3CN$ are shown in Figure 1a. The methyl ester forms of the compounds (**E1**–**E5**) displayed much slower kinetics for surface binding, requiring tens of hours to achieve the same surface coverage. The visible absorption spectra of the TiO_2 thin films sensitized with the ester forms of the compounds measured in 0.5 M $LiClO_4/CH_3CN$ are shown in Figure 1b. In both cases, the visible absortion spectra of the sensitized thin films, abbreviated **C#**/TiO_2 or **E#**/TiO_2, were very similar to those observed for the compounds in neat acetonitrile, indicating that the molecules anchored to the surface without measurable degradation.

Cyclic voltammetry of the sensitized thin films showed significant overlap of two redox waves with peak-to-peak splittings greater than 200 mV at a scan rate of 100 mV/s. Therefore, spectroelectrochemistry was carried out to estimate the reduction potentials and assign the redox processes. Figure 2 a,b shows representative UV–vis–NIR spectral changes upon oxidation for **C1**/TiO_2 and **C5**/TiO_2. Other data are shown in Figure S1 in the Supporting Information. Initial oxidation of **C1**/TiO_2 to **C1**$^+$/TiO_2 showed an absorption increase at 470 nm. Bleaches of the metal-to-ligand charge transfer (MLCT) bands at 433 and 531 nm indicated that oxidation occurred at the ruthenium metal center. The weak absorption band in the red and near-infrared region was attributed to ligand-to-metal

dx.doi.org/10.1021/ja410647c | J. Am. Chem. Soc. 2014, 136, 1034–1046

charge transfer (LMCT). Further oxidation beyond 1035 mV vs NHE resulted in the loss of the initial isosbestic points and the formation of new ones at 423 and 526 nm. A marked absorption band around 980 nm characteristic of $NAr_3^{\bullet+}$ absorption was observed that served as a probe of hole transfer in transient absorption studies. In the case of **C5**/TiO_2, the order of the redox chemistry was reversed. The immediate appearance of a strong absorption band from ~580 nm to the near-infrared region indicated that the first oxidation was NAr_3-centered.[2] This was followed by the ruthenium-centered oxidation at more positive potentials. The standard addition method based on global modeling was used to calculate the fraction of each species present at each applied potential, and representative values are shown as the insets in Figure 2. Overlaid on the data are sigmoidal fits, given by $x = 1/[1 + 10\exp(E_{app} - E^\circ)/a \times 59\ \text{mV}]$, where x is the fraction of molecules present at a given applied potential, a is the nonideality factor, and E° is the formal reduction potential of $Ru^{III/II}$ or $NAr_3^{\bullet+/0}$, taken as the applied potential where the concentrations of the oxidized and reduced forms were equal. These data are summarized in Table 1.

Theoretical characterization of three representative compounds (**C2**, **C4**, and **C5**) by density functional theory (DFT) was completed for the compounds in the ground and one-electron-oxidized states in the fully protonated form and with one of the carboxylic acid groups deprotonated. These calculations were performed to assess the molecular orbitals involved in the electron transfer chemistry and to quantify the change in dipole moment accompanying sensitizer oxidation. The frontier molecular orbitals are shown in Figures S2 and S3 in the Supporting Information. The HOMOs of the oxidized compounds are located over the phenyl rings of the NAr_3 donor, while the LUMOs are composed of orbitals on the terpyridyl rings with contributions from the Ru d orbitals. Shown in Figure 3 are the calculated dipole moment vectors for the ground and one-electron-oxidized states of **C2**, **C4**, and **C5** in the diprotonated form. The calculated dipole moment (μ) components are reported in Table S1 in the Supporting Information. It was found that the magnitudes of μ for the ground states of **C2**, **C4**, and **C5** were 27.4, 28.1, and 30.1 D, and after one-electron oxidation the dipole moments increased to 46.3, 50.8, and 55.5 D, respectively. The 9.2 D larger value for $\mathbf{C5}^+$ relative to $\mathbf{C2}^+$ resulted from the "hole" in $\mathbf{C5}^+$ being localized on the NAr_3 donor group rather than the metal center.

Nanosecond transient absorption spectroscopy was used to quantify the interfacial charge recombination between $TiO_2(e^-)$ and the oxidized compound. Figure 4 shows absorption difference spectra of the sensitized materials in an acetonitrile electrolyte at 100 ns delay time after 532 nm laser excitation. A single product was observed after laser excitation, consistent with excited-state injection and hole transfer occurring on a sub-10 ns time scale. At early observation times, evidence of a faster component was observed for **C5**/TiO_2, and measurements at −45 °C revealed a ~5 ns rise time for the appearance of the oxidized $NAr_3^{\bullet+}$ (Figure S4 in the Supporting Information). This process was within the instrument response time but indicated that hole transfer occurs on a time scale from hundreds of picoseconds to a few nanoseconds. A progressive increase in the absorption band in the red region attributed to $NAr_3^{\bullet+}$ was observed in going from **C1** to **C5** or from **E1** to **E5** that was correlated with the increase in the value of $[E^\circ(Ru^{III/II}) - E^\circ(NAr_3^{\bullet+/0})]$. The kinetics measured for charge recombination between the injected electrons and the oxidized dye molecules were in good agreement with the results for $\mathbf{C2}^+/TiO_2(e^-)$, $\mathbf{C4}^+/TiO_2(e^-)$, and $\mathbf{C5}^+/TiO_2(e^-)$ reported in an earlier communication.[8] In the present work, with an additional two sensitized films, it was again found that within experimental error there was no difference in the charge recombination rate constants, indicating that recombination was insensitive to the identity of the compound (Figure S5 in the Supporting Information). The influence of surface coverage was also quantified (Figure S6 in the Supporting Information). Decreasing the surface coverage from the saturation value (6×10^{-8} mol/cm^2) to values of ~1/5 saturation resulted in only a very minor change in the charge recombination kinetics.

Addition of sulfuric acid at concentrations as low as 1.0×10^{-4} M to a **C4**/TiO_2 thin film immersed in 0.5 M $LiClO_4$/CH_3CN induced a noticeable bathochromic shift and increase in the MLCT absorption band throughout the visible region (Figure 5). The spectral changes were preserved even after the

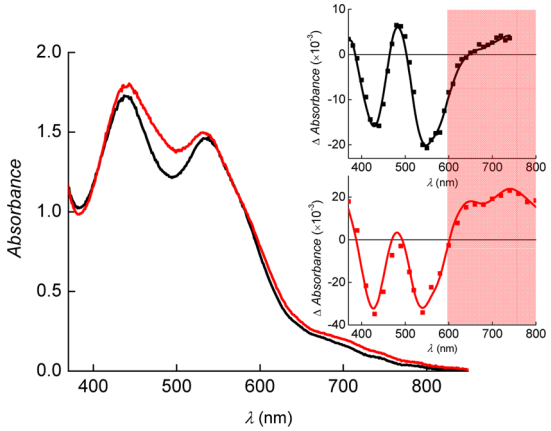

Figure 5. UV−vis absorption spectra of **C4**/TiO_2 immersed in 0.5 M $LiClO_4$/CH_3CN (black) and immersed in 0.5 M $LiClO_4$/1.0×10^{-4} M H_2SO_4/CH_3CN (red). The upper inset shows the absorption difference spectra measured 45 ns after pulsed 532 nm excitation of **C4**/TiO_2, and the lower inset shows the same data for an H_2SO_4-treated **C4**/TiO_2 thin film; overlaid in solid curves are simulations, and regions highlighted in pink are where $NAr_3^{\bullet+}$ absorbs strongly.

C4/TiO_2 thin film was reimmersed in fresh 0.5 M $LiClO_4$/CH_3CN. Laser excitation of the acid-exposed **C4**/TiO_2 thin film in 0.5 M $LiClO_4$/CH_3CN resulted in rapid excited-state electron injection to TiO_2 ($k_{inj} > 10^8$ s^{-1}). A significant absorption increase in the red region indicated a larger extent of intramolecular hole transfer relative to that for untreated **C4**/TiO_2 (Figure 5 insets). Spectral modeling indicated that the sulfuric acid treatment increased the hole transfer yield from 0.25 to 0.51. The ATR-FTIR spectra showed that the acid treatment resulted in the appearance of an intense carbonyl stretch at 1712 cm^{-1} that was at the same energy as that measured for a **C4** powder in the solid state (Figure S7 in the Supporting Information).

The presence of two stable oxidation states enabled studies where the Ru^{II} or NAr_3 group was oxidized prior to light excitation. Because of the proximity of the $Ru^{III/II}$ and $NAr_3^{\bullet+/0}$ reduction potentials for **C2**−**C5**, **C1** was chosen for the study as the reduction potentials were the most separated. The absorption difference spectra of **C1**/TiO_2 displayed in Figure 6a,c,e were acquired in 0.5 M $LiClO_4$/CH_3CN at applied potentials of 890, 960, and 1035 mV after 532 nm excitation. At

dx.doi.org/10.1021/ja410647c | J. Am. Chem. Soc. 2014, 136, 1034−1046

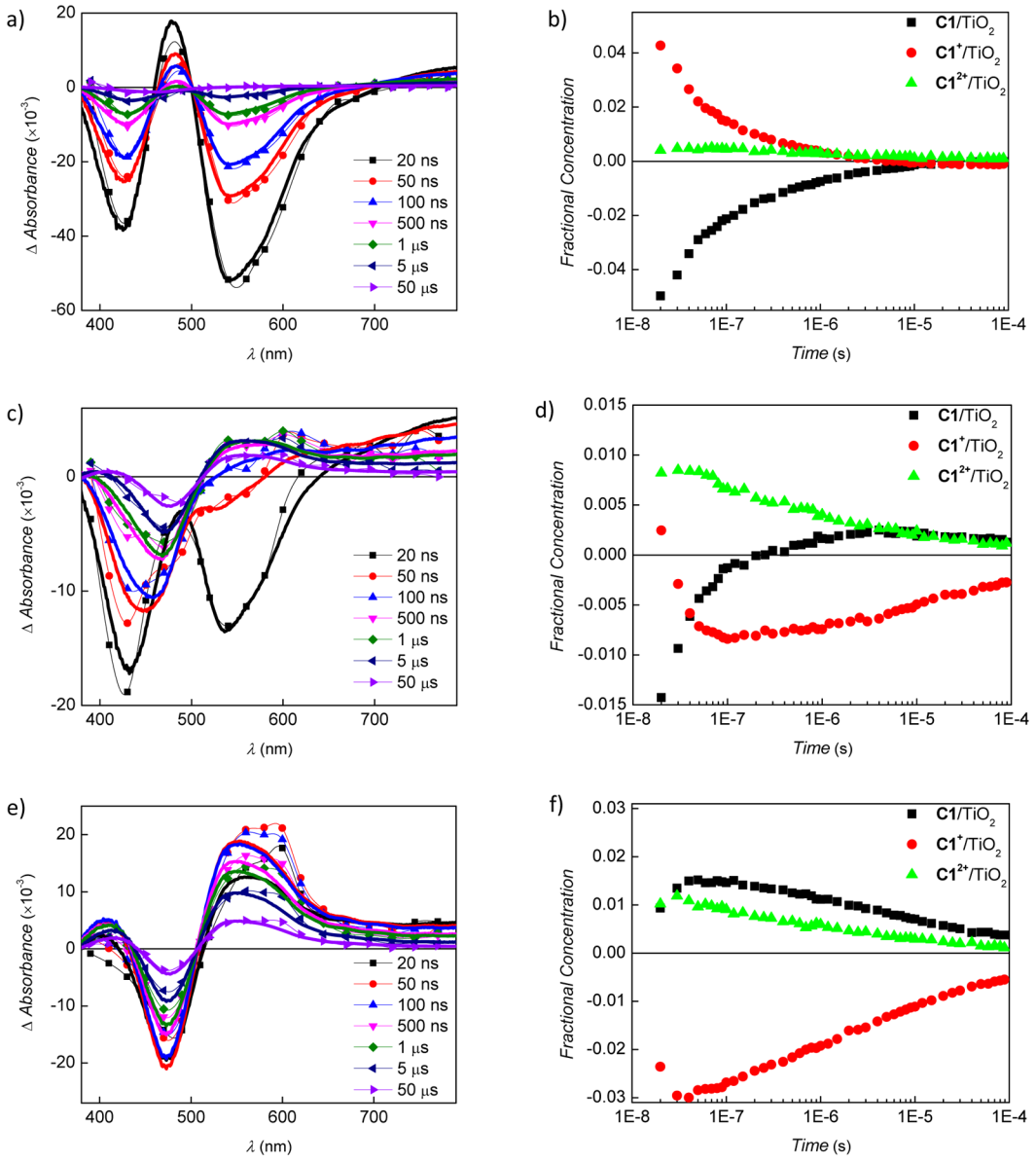

Figure 6. (a, c, e) Absorption difference spectra measured after pulsed laser excitation (λ_{ex} = 532 nm) of **C1**/TiO_2 biased to (a) 890 mV vs NHE (**C1**/TiO_2:**C1**$^+$/TiO_2 = 50:50), (b) 960 mV vs NHE (**C1**/TiO_2:**C1**$^+$/TiO_2 = 15:85), and (c) 1035 mV vs NHE (**C1**/TiO_2:**C1**$^+$/TiO_2 = 0:100) at the indicated delay times. Overlaid in solid lines are simulations based on the absorption profiles of **C1**/TiO_2, **C1**$^+$/TiO_2, and **C1**$^{2+}$/TiO_2 (shown in Figure S8 in the Supporting Information) and the first-derivative spectrum of **C1**$^+$/TiO_2 using the corresponding fractional concentrations of **C1**/TiO_2 (black squares), **C1**$^+$/TiO_2 (red circles), and **C1**$^{2+}$/TiO_2 (green triangles) as functions of time, shown in (b), (d), and (f).

these potentials, the ratios of sensitizers present prior to light excitation were calculated from the spectroelectrochemical data. Spectral modeling based on the measured absorption spectra of **C1**, **C1**$^+$, and **C1**$^{2+}$ (Figure S8 in the Supporting Information) and TiO_2(e^-) were necessary to simulate the measured spectra. Spectral shifts due to an underlying Stark effect were also evident, and inclusion of the first-derivative absorption spectrum of **C1**$^+$/TiO_2 improved the spectral modeling as has been previously described.[26,27] The fractions of **C1**, **C1**$^+$, and **C1**$^{2+}$ generated after 532 nm light excitation over the total number of molecules (**C1** + **C1**$^+$ + **C1**$^{2+}$) as functions of the delay time were deconvoluted from the time-resolved spectral data and are shown in Figure 6b,d,f. Because the concentration of each oxidation state was determined, the injection yield of **C1**$^+$/TiO_2 was calculated to be ~0.1 at a delay time of 20 ns (Figure 6b).

A single wavelength of 507 nm was chosen to monitor the interfacial charge recombination of TiO_2(e^-) with the oxidized sensitizers (Figure 7). The absorption changes as a function of time were satisfactorily described by the Kohlrausch–Williams–Watts (KWW) model (eq 1)[28,29] with a fixed

$$\Delta\mathrm{Abs} = A\,\exp[-(kt)^{\beta_{\mathrm{KWW}}}] \qquad (1)$$

β_{KWW} value of 0.17 under all bias conditions. The rate of this process was found to be dramatically increased when more oxidized compounds (i.e., more positive potentials) were generated on TiO_2 surfaces.

Shown in Figure 8 are time-resolved absorption data measured after pulsed laser excitation of a **C1**/TiO_2 thin film held at an applied bias of +1035 mV vs NHE. At this applied potential, the ruthenium center was oxidized to the formal

dx.doi.org/10.1021/ja410647c | J. Am. Chem. Soc. 2014, 136, 1034–1046

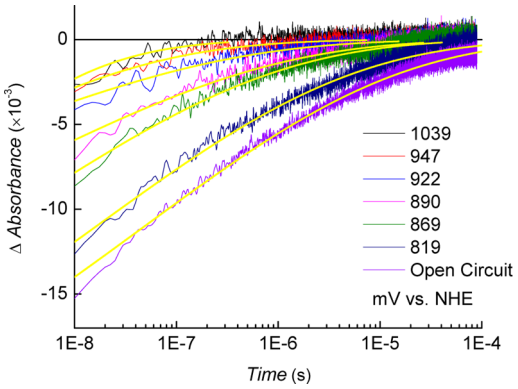

Figure 7. Absorption changes monitored at 507 nm after pulsed light excitation at the indicated applied potentials (λ_{ex} = 532 nm, 1.4 mJ/cm^2). Overlaid in yellow are the fits to the KWW model (β_{KWW} = 0.17).

oxidation state of +III and is therefore better formulated as $\mathbf{C1}^{+}$/TiO_2. Excited-state injection was rapid and efficient ($k_{inj} > 10^8$ s^{-1} and ϕ_{inj} = 0.1). The data were recorded at five different irradiances from 0.3 to 1.5 mJ/cm^2. Two different Monte Carlo simulation methods were used to understand the lateral intermolecular hole hopping process that occurred after interfacial electron transfer to a second dye molecule. In the first method, 536 dye molecules were evenly distributed on a single 15 nm diameter sphere with an average intermolecular distance of 11.5 Å. The second method took 27 similar spheres and packed them into a 2 × 2 × 2 or a 3 × 3 × 3 cubic array with nearest-neighbor center-to-center interparticle distances of 14.8 nm. In these arrays, dye molecules in the necking regions between spheres were removed. In both methods, after excited-state electron injection, the injected electron quantitatively recombined with a different molecule to yield equal numbers of **C1** and $\mathbf{C1}^{2+}$ randomly positioned on the surface. The random walk of each **C1** or $\mathbf{C1}^{2+}$ was controlled by a pseudorandom number generator either to the six adjacent $\mathbf{C1}^{+}$ sites with equal probability for one sphere or weighted exponentially (β = 0.35 Å^{-1})[30,31] by the distance to every other site. The $Ru^{III/II}$ and $NAr_3^{\bullet+/0}$ hopping rates were assumed to be the same, such that an "effective" hopping rate was calculated. This assumption was supported by the spectroelectrochemical data, which showed that the time required to oxidize 40% of the NAr_3 donors in **C5**/TiO_2 was only about 1.5 times shorter than that required to oxidize the same percentage of Ru^{II} sites in **C1**/TiO_2, implying that the hopping rates were indeed very similar. Hole transfer from $\mathbf{C1}^{2+}$ to **C1** to yield two $\mathbf{C1}^{+}$ compounds was assumed to be quantitative when the two were adjacent. For both methods, the initial number of **C1** and $\mathbf{C1}^{2+}$ molecules created with light was an important parameter that influenced the kinetic behavior for lateral hole hopping. Hole-hopping simulations for cases where one, two, three, four, or five charge-separated pairs were created on each TiO_2 particle as well as 27, 54, 81, 108, or 135 pairs for each 27 particle array were performed. The best fits of the simulation data to the experimental data as determined by χ^2 analyses (Figure S12 in the Supporting Information) are shown as the solid curves overlaid on the transient data in Figure 8. Hopping rates of (160 ns)$^{-1}$ for the single-particle case and (130 ns)$^{-1}$ for the particle arrays were found. Simulations based on the nanoparticle arrays gave rise to a more well-defined minimum and were found to be in better agreement with the experimental data, particularly those data measured on the longer time scales (Figures S11 and S12 in the Supporting Information).

DISCUSSION

The redox and photoinduced electron transfer properties of TiO_2 thin films sensitized with five different cyclometalated ruthenium compounds with conjugated triarylamine donor groups were quantified. The presence of two redox-active portions of these compounds, $Ru^{III/II}$ and $NAr_3^{\bullet+/0}$, provided new insights into interfacial redox reactions that could not have been obtained with a single chromophoric sensitizer. In the discussion below, emphasis is placed on published literature on solar energy conversion that relates to (1) the non-Nernstian nature of the interfacial redox chemistry, (2) intramolecular hole transfer, (3) dipole moment contributions to the stored Gibbs free energy, and (4) lateral intermolecular hole transfer across the TiO_2 surface.

Non-Nernstian Redox Chemistry. The Nernst equation predicts that for a one-electron transfer process at room temperature, a 59 mV shift in potential should arise when the ratio of the concentrations of the reduced and oxidized forms are changed by a factor of 10.[32] This relation has been phenomenally successful in fluid electrolyte solutions, particularly when activities are used in place of concentrations.[32] However, non-Nernstian behavior has been noted at chemically modified electrode surfaces and has been quantified by

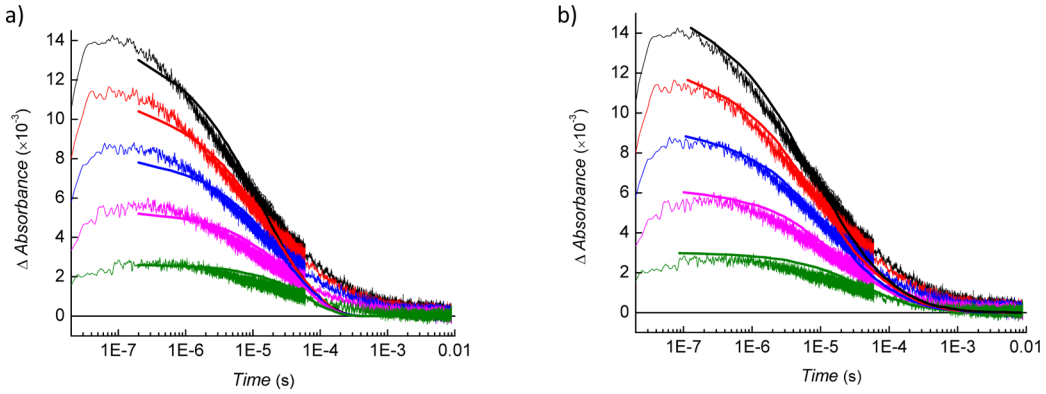

Figure 8. Absorption changes monitored at 540 nm after pulsed light excitation with five irradiances (λ_{ex} = 532 nm and 0.3−1.5 mJ/cm^2) of **C1**/TiO_2 immersed in 0.5 M $LiClO_4$/CH_3CN and biased at 1035 mV vs NHE. Overlaid as solid lines are absorption profiles abstracted from Monte Carlo simulations of (a) 1 and (b) 27 nanoparticles.

dx.doi.org/10.1021/ja410647c | J. Am. Chem. Soc. 2014, 136, 1034−1046

inclusion of a nonideality factor, a, into the Nernst equation.[10,11,33−35] When a = 1 in eq 2, the Nernst equation

$$E = E^{\circ} + \frac{aRT}{nF} \ln \frac{[\mathrm{Ox}]}{[\mathrm{Red}]} \quad (2)$$

results. Nonideality results when a > 1, behavior most often attributed to intermolecular interactions accompanying the redox chemistry as described by Frumkin.[36,37] The availability of two redox-active groups in these compounds, namely, the $Ru^{III/II}$ center and the $NAr_3^{\bullet+/0}$ group, which is expected to be further from the TiO_2 surface, enabled interrogation of the origin of the nonideality by spectroelectrochemistry.

It was found that in order to achieve a factor of 10 change in concentration, more than 59 mV of applied potential was needed, and hence, nonideality factors had to be introduced to model all of the interfacial electrochemical data. For instance, a nonideality factor a = 1.45 was measured for $Ru^{III/II}$ of **C1**/TiO_2, indicating that an ∼90 mV potential step was required for a factor of 10 change in concentration. Interestingly, the $Ru^{III/II}$ redox reactions for all five compounds revealed higher nonideality factors than those of the covalently linked $NAr_3^{\bullet+/0}$ groups (1.37 ± 0.08 vs 1.15 ± 0.09, respectively). The $Ru^{III/II}$ nonideality factors were larger than those of $NAr_3^{\bullet+/0}$ regardless of which redox center was oxidized first in the compound. For example, the ruthenium center was oxidized first in **C2** and second in **C5**, yet both displayed nonideality factors of ∼1.32. As counterions and solvent reorganize as a consequence of the redox chemistry, the insensitivity of the nonideality factors to the total oxidation state of the molecule implies that such interfacial reorganization was not the cause of the nonideality. It could well have been the case that the second group oxidized displayed the larger nonideality factors due to the higher charge on the molecule, but this was not observed.

The origin of the nonideality is instead consistent with either intermolecular interactions, as proposed by Frumkin,[36,37] or a surface electric field model.[38] The former seems less likely, as space-filling models indicate that the rigid thiophene linker results in similar Ru−Ru and NAr_3−NAr_3 intermolecular distances. Therefore, the surface electric field experienced by the redox-active group is most likely the origin of the nonideality, as such fields are known to decrease with distance from the semiconductor surface.[33,38,39] The only previously related literature report was a recent study of a cobalt porphyrin anchored to TiO_2, where both $Co^{III/II}$ and $Co^{II/I}$ reactions were quantified.[33] While this chemistry was complicated somewhat by coordination number changes that accompany this redox chemistry, larger nonideality factors were observed for $Co^{II/I}$ relative to $Co^{III/II}$. Like the $Ru^{III/II}$ and $NAr_3^{\bullet+/0}$ redox chemistry reported herein, the $Co^{III/II}$ redox potentials occurred within the forbidden band gap of TiO_2 and hence required a percolation pathway from the transparent conductive substrate to the molecules (see Intermolecular Hole Hopping below), while the direct reduction of TiO_2 accompanied the conversion of Co^{II} to Co^{I}. Electrons injected into TiO_2 produce a large electric field, E = 3 MV/cm, that has been observed by electroabsorption spectroscopy (i.e., Stark spectroscopy) and reported to be distance-dependent.[26,39−41] Hence, the enhanced nonideality factors reported for $Co^{II/I}$ redox chemistry were also attributed to a surface electric field, consistent with the conclusions drawn here.

The appearance of nonideal redox chemistry raises the issue of what the true reduction potentials of the surface-anchored compounds are. This question is particularly relevant to operational solar cells when an electric field mechanism for nonideality is operative, as the reduction potentials would no longer be fixed values and would instead change with the solar flux. For the purposes of this study, the formal reduction potential was taken as the potential where the equilibrium concentrations of the oxidized and reduced forms were equal, with the understanding that these potentials likely do shift to more negative values with the TiO_2 quasi-Fermi level under solar illumination. Comparisons of these "dark" potentials with those measured for the free compounds in fluid electrolytes were difficult because the carboxylic acid forms of the compounds were nearly insoluble in CH_3CN. However, the ester derivatives were soluble, and the $NAr_3^{\bullet+/0}$ reduction potentials measured were in good agreement with the interfacial values. In contrast, the $Ru^{III/II}$ potentials were generally 70−90 more positive than those measured at the TiO_2 interface. This shift is consistent with an inductive effect where the electron-donating carboxylate binding groups yield less positive $Ru^{III/II}$ potentials than do the electron-withdrawing ester groups. Thus, the formal reduction potentials do not appear to be significantly altered upon surface binding once the change from carboxylic acid (or ester) to carboxylate that accompanies surface binding is taken into account. Nevertheless, the nonideality of the molecular redox chemistry at the TiO_2 interface perturbs the equilibrium for intramolecular hole transfer in a quantifiable manner as described below.

Intramolecular Hole Transfer. It was of interest to calculate the extent of hole transfer from the oxidized ruthenium center to the covalently linked triarylamine moiety on the basis of the spectroelectrochemical data, as these values can be compared to those measured experimentally after pulsed laser excitation. To account for the nonidealities and to be consistent with the spectroelectrochemical results, the $Ru^{III/II}$ and $NAr_3^{\bullet+/0}$ redox reactions were considered to be independent of each other even though these moieties were covalently linked (eq 3).[42] The equilibrium constants and hole transfer yields were calculated with eqs 4 and 5, respectively. The hole transfer yields without and with the inclusion of

Table 1. Electrochemical and Photophysical Data for the Sensitized Thin Films

	$E^{\circ}_{1/2}(Ru^{III/II})^a$ $(a_1)^b$	$E^{\circ}_{1/2}(NAr_3^{\bullet+/0})^a$ $(a_2)^b$	$K_{eq}{}^c$	$\Phi_{ht,calc}$	$\Phi_{ht,a}$	$\Phi_{ht,meas}$	$E^{\circ}_{1/2}(Ru^{III/II*})$ (V)	ΔG_{es} (eV)^d	abs max (nm)
C1	890 (1.45 ± 0.04)	1155 (1.22 ± 0.04)	3.31×10^{-5}	<0.01	0.02	<0.02^e	−0.76	1.65	435, 534
C2	945 (1.30 ± 0.04)	1150 (1.21 ± 0.04)	3.42×10^{-3}	0.02	0.04	<0.02^e	−0.72	1.65	431, 529
C3	1010 (1.44 ± 0.03)	1150 (1.24 ± 0.02)	4.30×10^{-3}	0.06	0.12	0.05^e	−0.67	1.68	427, 519
C4	870 (1.33 ± 0.03)	960 (1.11 ± 0.03)	3.01×10^{-2}	0.15	0.19	0.25	−0.81	1.68	439, 532
C5	1060 (1.33 ± 0.04)	940 (1.04 ± 0.03)	1.07×10^{2}	0.91	0.88	0.74	−0.62	1.68	431, 520

$^a E^{\circ}_{1/2}$ given in mV vs NHE. $^b a_1$ and a_2 are the nonideality factors in eqs 3 and 4. $^c K_{eq}$ is defined in eq 4. $^d \Delta G_{es}$ was estimated from the corrected photoluminescence spectrum measured for sensitized ZrO_2. ^{e}Estimated from the absorption amplitude at 720−750 nm relative to **C5**/TiO_2.

dx.doi.org/10.1021/ja410647c | J. Am. Chem. Soc. 2014, 136, 1034−1046

Scheme 4. Chemical Capacitance of (a) C3/TiO_2 and (b) C5/TiO_2 as a Function of Applied Potential[a]

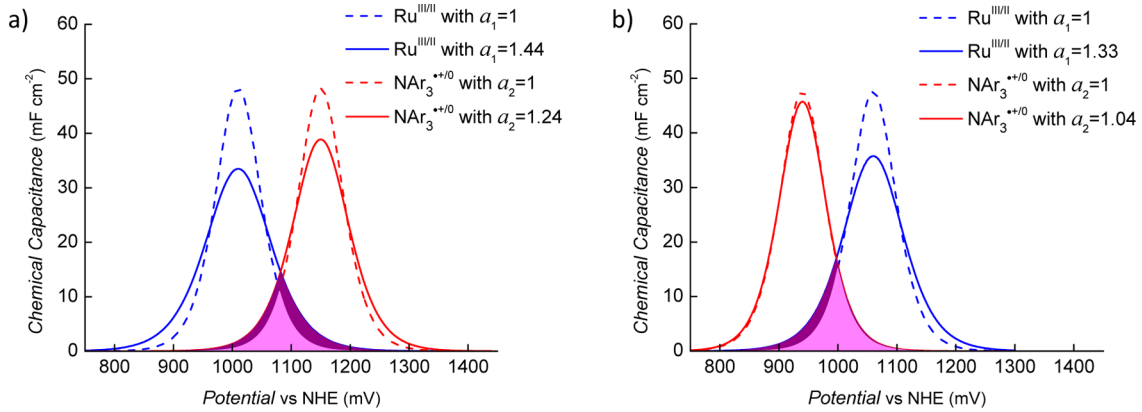

[a]The solid curves represent best fits to the experimental data with the indicated nonideality factors. The dashed curves represent ideal Nernstian behavior. The overlap of the chemical capacitance represents potentials where both triarylamine and ruthenium redox chemistry occurs.

nonideality factors (Φ_{calc} and $\Phi_{calc,a}$, respectively) were calculated, where a_1 and a_2 represent the nonideality factors for $Ru^{III/II}$ and $NAr_3^{\bullet+/0}$, respectively. The results are summarized in Table 1.

$$Ru^{III} + NAr_3 \overset{K_{eq}}{\rightleftharpoons} Ru^{II} + NAr_3^{\bullet+} \quad (3)$$

$$K_{eq} = \frac{[Ru^{II}]^{a_1}[NAr_3^{\bullet+}]^{a_2}}{[Ru^{III}]^{a_1}[NAr_3^{0}]^{a_2}} \quad (4)$$

$$\Phi_{ht,calc} = \frac{[NAr_3^{\bullet+}]}{[NAr_3^{0}] + [NAr_3^{\bullet+}]} = \frac{K_{eq}^{1/(a_1+a_2)}}{1 + K_{eq}^{1/(a_1+a_2)}} \quad (5)$$

The inclusion of nonideality factors in essence broadens the potential range over which $Ru^{III/II}$ and $NAr_3^{\bullet+/0}$ redox chemistry occurs. This is conveniently depicted through the chemical capacitance as first suggested by Murray (Scheme 4).[35] Three different scenarios are possible for the hole transfer reaction under study. In the first, the driving force for hole transfer is small and $K_{eq} \ll 1$. This is the case for **C3**/TiO_2 ($K_{eq} = 4.3 \times 10^{-3}$), and the inclusion of nonideality factors increases the overlap region and hence the fraction of Ru^{III} that can oxidize the NAr_3 group (Scheme 4a). Hence, nonideality is expected to increase the yield of hole transfer after excited-state injection when $K_{eq} \ll 1$. For **C3**/TiO_2 the magnitude of the effect was about a factor of 2. The second scenario occurs when $K_{eq} = 1$, where little change in the yield of hole transfer is expected provided that the nonideality factors are similar. The third scenario occurs when the driving force for hole transfer is large and $K_{eq} \gg 1$, as was found to be the case for **C5**/TiO_2 ($K_{eq} = 1.1 \times 10^2$). Here the inclusion of nonideality factors results in a larger fraction of NAr_3 groups that cannot be oxidized by Ru^{III} (Scheme 4b). As a result, the expected hole transfer quantum yield decreases, by about 16% in the case of **C5**/TiO_2.

The quantum yields for hole transfer measured after pulsed laser excitation of the sensitized thin films were in better agreement with the calculated values when the nonideality factors were included, particularly for **C4**/TiO_2 and **C5**/TiO_2, which displayed hole transfer yields greater than 0.25. Therefore, as shown through steady-state equilibrium measurements and transient kinetic studies, nonideal redox behavior is detrimental for hole transfer when the Gibbs free energy change for the reaction is favorable. It should be kept in mind that the hole transfer yields were calculated from data measured in the absence of injected electrons while the experimental data were measured after excited-state electron transfer, where the injected electron itself was expected to give rise to nonideal behavior. Had the nonideality resulted from intermolecular interactions (i.e., Frumkin-like behavior), one might anticipate that it would be absent in the photoinduced charge separation studies, where the number of oxidized dye molecules is small, on average less than five per nanocrystallite. Therefore, this suggests that nonidealities need to be taken into account for prediction of hole transfer yields and that the nonideality is likely due to the surface electric field.

The yield for photoinduced intramolecular hole transfer measured experimentally was highly sensitive to the interfacial conditions, as both increased proton concentration and the presence of ester groups resulted in enhanced hole transfer yields. The methyl ester derivatives of the sensitizers were found to anchor to the TiO_2 surface with a pronounced ATR-FTIR absorption peak at 1730 cm^{-1} indicative of unhydrolyzed methyl ester groups. Enhanced hole transfer yields were measured for thin films sensitized with these compounds relative to the corresponding carboxylic acid derivatives. This can be rationalized by the inductive electron-withdrawing nature of the unhydrolyzed ester groups relative to the electron-donating carboxylate groups present on the TiO_2 surface. Indeed, the same behavior was observed after protonation of free carboxylate groups by a dilute H_2SO_4/CH_3CN solution. For example, light excitation of acid-treated **C4**/TiO_2 resulted in a factor of 2 increase in the hole transfer yield. These data show that the hole transfer yield was highly sensitive to environmental conditions such as the interfacial pH.

The Role of Dipole Moments. Charge recombination from $TiO_2(e^-)$ to the oxidized compounds was insensitive to whether the hole was localized on Ru^{III} or $NAr_3^{\bullet+}$. Therefore, for these compounds there was no kinetic advantage gained by hole transfer from Ru to the NAr_3 group. An explanation for this behavior remains unknown, but it may emanate from the conjugated thiophene bridge that links the triarylamine to the cyclometalated ligand, which provides a delocalized LUMO with metal d and NAr_3 orbital character for all of the compounds studied. Back electron transfer to the Ru center may hence always occur. This would also be expected to occur when the redox equilibrium shown in Scheme 2 is established

dx.doi.org/10.1021/ja410647c | J. Am. Chem. Soc. 2014, 136, 1034−1046

on the electron transfer time scale: the injected electron reduces Ru^{III}, shifting the equilibrium to the left, and hence more Ru^{III} is generated. Kinetic evidence that the quasi-intramolecular redox equilibrium was established on the time scale before back interfacial electron transfer comes from the fact that the hole transfer rate constant for $Ru^{III} \rightarrow NAr_3$ occurred on a time scale shorter than $k_{ht} \geq 1 \times 10^8\ s^{-1}$ for all of the sensitized materials while recombination required milliseconds.

Regardless of the mechanism, charge recombination of the injected electron with the oxidized sensitizer was remarkably insensitive to the sensitizer employed. At the same time, the open-circuit voltage (V_{oc}) measured in the absence of a redox mediator was approximately 100 mV larger for **C5**/TiO_2, which displayed the highest quantum yield for hole transfer to the amine donor. This was unexpected, as the spectroelectrochemical data showed that the acceptor states in TiO_2 were insensitive to the identity of the dye molecules present on the surface and hole transfer results in a *loss* in free energy. Therefore, if anything, hole transfer should have given rise to a smaller V_{oc} for **C2**/TiO_2 than for **C5**/TiO_2. In many previous studies, a decrease in the charge recombination rate constant compensated for this loss in free energy, as predicted by the diode equation.[9] However, an ~100 fold diminution of this rate constant would be needed to account for the measured V_{oc} values, and this simply was not observed. Other factors such as inefficient sensitizer regeneration,[6,27,43] acid–base chemistry,[44] and/or interfacial dipole moments of the ground-state dyes are also known to influence V_{oc}.[45−47]

It is asserted that the enhancement in V_{oc} reported here results from the increased dipole moment that accompanies hole transfer. This assertion comes in part from an elimination of all other possibilities such as the recombination kinetics described above. Furthermore, spectroelectrochemical studies showed that the TiO_2 density of acceptor states was insensitive to the identity of the dye molecule and hence that specific sensitizer effects, such as the protonation state of the dye molecule as reported by Nazeeruddin and co-workers,[44] were not operative in this homologous series of dye molecules. In addition, it has previously been shown that the orientation of molecular dipole moments at the TiO_2 surface influences V_{oc} through the electrostatic field generated.[48,49] Dipoles oriented toward the surface increase V_{oc} because of the upshift of the quasi-Fermi level of the TiO_2 nanoparticle, while those directed away decrease V_{oc}. Before comparing these experimental data to the results of previous studies, it is important to point out a key experimental detail: the open-circuit photovoltage data reported here was measured against a pseudoreference electrode in the absence of redox mediators, while most other literature reports are for an operational solar cell with a redox mediator present, typically I^-/I_3^-. For this reason, previous workers used the inherent dipole of the surface-anchored dye molecule, or coadsorbed nonchromophoric dipolar molecules, and attributed the measured V_{oc} to the ground state, that is, the nonilluminated thin film.[45−48] This was reasonable as the steady-state concentrations of excited and oxidized sensitizers were thought to be vanishingly small and hence would not contribute to the measured V_{oc} values. In contrast, the data reported here were very sensitive to the concentration of the oxidized dye molecules as no regenerator was present. When the sensitized thin films were illuminated in such a nonregenerative cell, oxidized dye molecules were formed along with injected electrons that raised the TiO_2 quasi-Fermi level toward the vacuum level. These oxidized states had dipole moments that were almost twice as large as those of their ground states, as shown by DFT calculations. In addition, the calculated dipole moments were largest when the hole was predominantly localized on the NAr_3 group. For example, $Ru^{III} \rightarrow NAr_3$ hole transfer in **C5**$^+$/TiO_2 gave rise to a 9.2 D increase in dipole moment relative to **C2**$^+$/TiO_2, where the hole was predominantly localized on the Ru^{III} center.

The dipole moment data can be used to calculate the dipole-moment-induced electrostatic potential drop ($\Delta\phi_{dipole}$), eq 6.

$$\Delta\phi_{dipole} = \frac{N\Delta(\mu \cos\theta)}{\varepsilon\varepsilon_0} \tag{6}$$

This equation predicts that the V_{oc} should be dependent on the change in the surface dipole moment that accompanies excited-state injection, $\Delta(\mu \cos\theta)$, and the surface coverage of oxidized molecules, N, assuming that the permittivity of the molecular layer $\varepsilon = 5$.[48] At most about 10% of the dye molecules injected electrons at the highest irradiance employed, so N would be ~7×10^{16} molecules/m^2. When the full range of tilt angles and dipole moments of different protonation states of the dye molecule were considered (see Table S1 in the Supporting Information), a $\Delta\phi_{dipole}$ range of 40−60 mV was calculated to accompany hole transfer, which is in reasonable agreement with the value of 100 mV measured experimentally.

One could rightly argue that the V_{oc} data reported here have little relevance to an operational dye-sensitized solar cell, which necessarily contains a redox mediator. With some organic dye molecules, however, compelling evidence was found that inefficient sensitizer regeneration lowers V_{oc}.[27] Hence, some fraction of the injected electrons leak back to the oxidized dye molecule under conditions where the number of injected electrons is large. More recently, Wang and co-workers reported clear evidence that this also occurs for highly optimized dye molecules like $Ru(dcbH_2)(dnb)(NCS)_2$ (Z907), where $dcbH_2$ is 4,4′-$(CO_2H)_2$-2,2′-bipyridine and dnb is 4,4′-dinonylbipyridine.[43] In one previous comparative study of donor–acceptor-sensitized thin films where the charge recombination kinetics was correlated with the kinetics for back interfacial electron transfer to the oxidized donor, the enhanced V_{oc} that accompanied hole transfer was measured in the presence and absence of the redox mediator.[1] Taken together, these results indicate that one cannot rule out the possibility that dipole moment measurements made without a redox mediator do have some relevance to operational solar cells. In any event, measurements of V_{oc} in the absence of redox mediators are the most useful for fundamental studies of the interfacial dipole moment changes that follow excited-state injection.

Intermolecular Hole Hopping. It has long been known that molecules with formal reduction potentials that lie within the forbidden band gap, where TiO_2 is expected to be an insulator, can be reversibly oxidized in these mesoporous thin films.[50] The established mechanism is that oxidation is initiated at the transparent conductive oxide (TCO) substrate and proceeds by lateral intermolecular hole hopping throughout the film provided that a percolation threshold has been achieved.[51,52] Recently, lateral hole hopping has also been observed to occur after excited-state injection by time-resolved anisotropy spectroscopic measurements.[31] The sensitized interfaces under study here enabled lateral hole hopping reactions to be induced with light and monitored by transient

absorption spectroscopy (Scheme 5). Such reactions are important in photoelectrosynthetic cells as they provide a means for translating oxidizing equivalents to a catalyst after excited-state injection.

Scheme 5. Electron Transfer and Hole Hopping Processes Observed after 532 nm Laser Excitation of $C1^+/TiO_2$: (a) Excited-State Electron Injection; (b) Interfacial Charge Recombination; (c) Lateral Intermolecular Hole Hopping

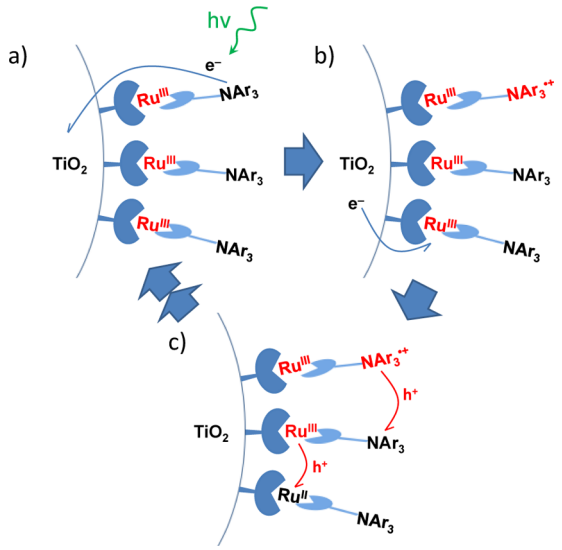

When the Ru^{II} center in $C1/TiO_2$ was electrochemically oxidized to yield $C1^+/TiO_2$ (i.e., Ru^{III}–NAr_3), a new visible absorption band centered at 470 nm was observed that was assigned to be an intraligand charge transfer band from the triarylamine donor to the substituted terpyridine ligand (NAr_3 → terpy*). This band is very similar in energy and bandwidth to that observed for organic D–π–A molecules with triarylamine donors.[27] In addition, DFT calculations of the one-electron-oxidized forms of these compounds revealed that the HOMO is largely centered on the NAr_3 group and the LUMO on the terpyridyl ligand (Figure S3 in the Supporting Information). Light excitation into this band resulted in the immediate appearance of the doubly oxidized sensitizer (i.e., where both Ru and NAr_3 were oxidized), confirming excited-state electron injection into TiO_2 from $C1^+$ (Scheme 5a and eq 7). The interfacial electron injection yield measured by

$$TiO_2|Ru^{III}\text{–}NAr_3 \xrightarrow{h\nu} TiO_2(e^-)|Ru^{III}\text{–}NAr_3^{\bullet+} \quad (7)$$

comparative actinometry on a 50 ns time scale was 0.1. It was unclear whether this low yield resulted from rapid back electron transfer or from intramolecular reductive quenching by the proximate Ru^{III} center followed by rapid back electron transfer.

Excited-state electron injection was followed by interfacial back electron transfer to a neighboring $C1^+$ molecule (eq 8).

$$TiO_2(e^-)|Ru^{III}\text{–}NAr_3 \rightarrow TiO_2|Ru^{II}\text{–}NAr_3 \quad (8)$$

This process was investigated as a function of applied bias, which created different concentrations of singly oxidized **C1**. It was found that charge recombination rates were much larger when oxidized compounds were present. Kinetic modeling did not show a simple relationship between the rate constants abstracted from a KWW analysis and the concentration of the oxidized dye molecules. However, at one extreme where all of the compounds were oxidized, the KWW rate constants were 3 orders of magnitude larger than those under the conditions where no dye molecules had been electrochemically oxidized. The increased charge recombination was due to a higher probability of the injected electron to encounter a $C1^+/TiO_2$. Quantitative interfacial back electron transfer in principle yielded $C1/TiO_2$ and $C1^{2+}/TiO_2$ in equal concentrations.

Hole transfer from $C1^{2+}/TiO_2$ to $C1/TiO_2$ (eq 9) was favored by 270 mV of Gibbs free energy and occurred after

$$TiO_2|Ru^{III}\text{–}NAr_3^{\bullet+} + TiO_2|Ru^{II}\text{–}NAr_3 \rightarrow 2(TiO_2|Ru^{III}\text{–}NAr_3) \quad (9)$$

lateral intermolecular $Ru^{III/II}$ and $NAr_3^{\bullet+/0}$ hole hopping across the TiO_2 surface brought the two reactants close to each other. A significant absorption change accompanied this recombination reaction process that could not be adequately described by first- or second-order kinetic models. Instead, the data were fit to a random walk model based on Monte Carlo simulations. Scheme 6a shows a representative Monte Carlo simulation of

Scheme 6. Monte Carlo Simulations of Lateral Intermolecular Hole Hopping on Spherical TiO_2 Nanocrystallites: (a) Single TiO_2 Particle; (b) Array of 27 TiO_2 Particles[a]

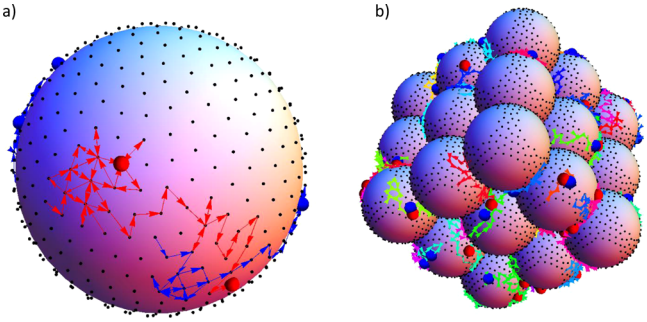

[a]Black dots represent the $C1^+$ sites that are evenly distributed on the surface. Red spheres are $C1^{2+}$ and blue spheres are **C1**. Thirty steps of random walks are shown.

three **C1** molecules (small blue spheres) and three doubly oxidized $C1^{2+}$ molecules (small red spheres) randomly positioned on a 15 nm diameter TiO_2 nanocrystal (large sphere). Time-dependent concentrations were calculated as the intermolecular hopping rate was varied, and the results were compared to experimental data measured at five different excitation irradiances. The simulations agreed with experiment when an effective intermolecular hole hopping rate of $(160\ ns)^{-1}$ was used. The experimental and simulated data were in best agreement on the microsecond and shorter time scales that represented greater than 70% of the recombination. The poor agreement on longer time scales might arise from cases where interparticle hopping occurred.[53] The necking regions could allow lateral hole hopping from one TiO_2 nanoparticle to another, thus decreasing the recombination rate. To test this hypothesis, an array of eight or 27 particles was used in a similar simulation that allowed for interparticle hopping (Scheme 6b).

dx.doi.org/10.1021/ja410647c | J. Am. Chem. Soc. 2014, 136, 1034–1046

The best fit of the simulation data to the experiment was achieved with an effective hopping rate of $(130\ \text{ns})^{-1}$. A χ^2 error analysis of the respective fits showed significant improvement of the multiparticle simulation over the single-particle simulation, and the residuals revealed that it was the longer-time-scale data where the fit to experimental data was most improved (Figure S12 in the Supporting Information). On average, the hole hopped about 16 nm before encountering a reduced compound. Because of the random nature of the walk, a total distance of ∼1800 nm would be reached if the path could be directed in a single direction.

The $(130\ \text{ns})^{-1}$ hopping rate recovered has relevance to photoelectrosynthetic water-splitting cells where accumulation of oxidizing equivalents at catalytic sites is required.[54−57] In one embodiment of such cells, the hole must hop to an oxidation catalyst after excited-state injection. This hole hopping is kinetically competitive with back electron transfer. At the lowest irradiance conditions studied, and with an average charge recombination rate constant of $2 \times 10^5\ \text{s}^{-1}$, a single oxidizing equivalent could circumnavigate a single nanocrystallite once in search of a catalyst before recombination. Unfortunate for this goal was the finding that charge recombination occurred on the same time scale as did hole hopping when every sensitizer had been oxidized by one electron. In this case, back electron transfer and efficient accumulation at a catalyst would not be expected. This finding emphasizes the need to isolate the catalyst from the TiO_2 surface for the realization of efficient photoelectrosynthetic cells.

■ CONCLUSIONS

The characterization of TiO_2 sensitized to visible light with molecules possessing two redox-active groups has provided new insights into the kinetics and thermodynamics of interfacial electron and hole transfer reactions. The redox chemistry was non-Nernstian, behavior reasonably attributed to the electric field present at the interface, and accounted for the hole transfer yields measured after pulsed laser excitation. The charge recombination kinetics and the density of TiO_2 acceptor states were the same for all of the sensitized materials that were characterized, while the open-circuit photovoltage was largest for the sensitizer that displayed the highest yield for hole transfer, demonstrating the importance of the dipole moment of the oxidized sensitizer. Finally, a novel photoinitiated intermolecular hole transfer process occurred with a hole hopping rate of $(130\ \text{ns})^{-1}$ that was sufficient to translate the hole a considerable distance from the site of excited-state injection, provided that the concentration of holes was small.

■ ASSOCIATED CONTENT

Supporting Information

Additional spectroelectrochemical data, molecular dipole moments, frontier molecular orbitals, charge recombination data, ATR-FTIR results, V_{oc} data, and χ^2 analysis/residuals plot of Monte Carlo simulations for lateral hole transfer reactions. This material is available free of charge via the Internet at http://pubs.acs.org.

■ AUTHOR INFORMATION

Corresponding Authors

rarratia@unab.cl
cberling@chem.ubc.ca
gjmeyer@unc.edu

Present Addresses

C.P.B.: Departments of Chemistry and Chemical & Biological Engineering, The University of British Columbia, Vancouver, BC V6T1Z1.
G.J.M.: The University of North Carolina at Chapel Hill, Chemistry Department, CB 3290, Chapel Hill, NC 27599-3290.

Notes

The authors declare no competing financial interest.

■ ACKNOWLEDGMENTS

G.J.M., K.H., and E.E.B. acknowledge support by a grant from the Division of Chemical Sciences, Office of Basic Energy Sciences, Office of Energy Research, U.S. Department of Energy (DE-FG02-96ER14662). K.H. acknowledges a Johns Hopkins University Harry and Cleio Greer Fellowship. C.P.B. and K.C.D.R. are grateful to the Canadian Natural Science and Engineering Research Council, Canadian Foundation for Innovation, Alberta Ingenuity, and the Canada School of Energy and Environment (CSEE) for support. E.S., X.Z., and R.A.-P. thank FONDECYT 1110758, 1130707, P07-006-F de la Iniciativa Científica Milenio del Ministerio de Economía, Fomento y Turismo.

■ REFERENCES

(1) Argazzi, R.; Bignozzi, C. A.; Heimer, T. A.; Castellano, F. N.; Meyer, G. J. *J. Am. Chem. Soc.* **1995**, *117*, 11815.
(2) Bonhôte, P.; Moser, J.-E.; Humphry-Baker, R.; Vlachopoulos, N.; Zakeeruddin, S. M.; Walder, L.; Grätzel, M. *J. Am. Chem. Soc.* **1999**, *121*, 1324.
(3) Hirata, N.; Lagref, J. J.; Palomares, E. J.; Durrant, J. R.; Nazeeruddin, M. K.; Grätzel, M.; Di Censo, D. *Chem.—Eur. J.* **2004**, *10*, 595.
(4) Haque, S. A.; Handa, S.; Peter, K.; Palomares, E.; Thelakkat, M.; Durrant, J. R. *Angew. Chem., Int. Ed.* **2005**, *44*, 5740.
(5) Staniszewski, A.; Heuer, W. B.; Meyer, G. J. *Inorg. Chem.* **2008**, *47*, 7062.
(6) McCall, K. L.; Morandeira, A.; Durrant, J.; Yellowlees, L. J.; Robertson, N. *Dalton Trans.* **2010**, *39*, 4138.
(7) Ashford, D. L.; Song, W.; Concepcion, J. J.; Glasson, C. R. K.; Brennaman, M. K.; Norris, M. R.; Fang, Z.; Templeton, J. L.; Meyer, T. J. *J. Am. Chem. Soc.* **2012**, *134*, 19189.
(8) Hu, K.; Robson, K. C. D.; Johansson, P. G.; Berlinguette, C. P.; Meyer, G. J. *J. Am. Chem. Soc.* **2012**, *134*, 8352.
(9) Ardo, S.; Meyer, G. J. *Chem. Soc. Rev.* **2009**, *38*, 115.
(10) Bisquert, J.; Garcia-Belmonte, G.; Garcia-Canadas, J. *J. Chem. Phys.* **2004**, *120*, 6726.
(11) Bisquert, J.; Fabregat-Santiago, F.; Mora-Seró, I.; Garcia-Belmonte, G.; Barea, E. M.; Palomares, E. *Inorg. Chim. Acta* **2008**, *361*, 684.
(12) Robson, K. C. D.; Sporinova, B.; Koivisto, B. D.; Schott, E.; Brown, D. G.; Berlinguette, C. P. *Inorg. Chem.* **2011**, *50*, 6019.
(13) Argazzi, R.; Bignozzi, C. A.; Heimer, T. A.; Castellano, F. N.; Meyer, G. J. *Inorg. Chem.* **1994**, *33*, 5741.
(14) Pavlishchuk, V. V.; Addison, A. W. *Inorg. Chim. Acta* **2000**, *298*, 97.
(15) *Amsterdam Density Functional (ADF) Code*, release 2009.01; Vrije Universiteit: Amsterdam, 2009.
(16) van Lenthe, E.; Snijders, J. G.; Baerends, E. J. *J. Chem. Phys.* **1996**, *105*, 6505.
(17) van Lenthe, E.; Baerends, E. J.; Snijders, J. G. *J. Chem. Phys.* **1994**, *101*, 9783.
(18) te Velde, G.; Bickelhaupt, F. M.; Baerends, E. J.; Fonseca Guerra, C.; van Gisbergen, S. J. A.; Snijders, J. G.; Ziegler, T. *J. Comput. Chem.* **2001**, *22*, 931.

(19) Snijders, J. G.; Vernooijs, P.; Baerends, E. J. *At. Data Nucl. Data Tables* **1981**, *26*, 483.
(20) van Lenthe, E.; Baerends, E. J. *J. Comput. Chem.* **2003**, *24*, 1142.
(21) Versluis, L.; Ziegler, T. *J. Chem. Phys.* **1988**, *88*, 322.
(22) Becke, A. D. *Phys. Rev. A* **1988**, *38*, 3098.
(23) Perdew, J. P. *Rhys. Rev. B* **1986**, *33*, 8822.
(24) Klamt, A. *J. Phys. Chem.* **1995**, *99*, 2224.
(25) Klamt, A.; Jonas, V. *J. Chem. Phys.* **1996**, *105*, 9972.
(26) Ardo, S.; Sun, Y.; Staniszewski, A.; Castellano, F. N.; Meyer, G. J. *J. Am. Chem. Soc.* **2010**, *132*, 6696.
(27) Robson, K. C. D.; Hu, K.; Meyer, G. J.; Berlinguette, C. P. *J. Am. Chem. Soc.* **2013**, *135*, 1961.
(28) Williams, G.; Watts, D. C. *Trans. Faraday Soc.* **1970**, *66*, 80.
(29) Lindsey, C. P.; Patterson, G. D. *J. Chem. Phys.* **1980**, *73*, 3348.
(30) Trammell, S. A.; Yang, J.; Sykora, M.; Fleming, C. N.; Odobel, F.; Meyer, T. J. *J. Phys. Chem. B* **2001**, *105*, 8895.
(31) Ardo, S.; Meyer, G. J. *J. Am. Chem. Soc.* **2011**, *133*, 15384.
(32) Bard, A. J.; Faulkner, L. R. *Electrochemical Methods: Fundamentals and Applications*, 2nd ed.; Wiley: New York, 2001.
(33) Ardo, S.; Achey, D.; Morris, A. J.; Abrahamsson, M.; Meyer, G. J. *J. Am. Chem. Soc.* **2011**, *133*, 16572.
(34) Albery, W. J.; Boutelle, M. G.; Colby, P. J.; Hillman, A. R. *J. Electroanal. Chem. Interfacial Electrochem.* **1982**, *133*, 135.
(35) Smith, D. F.; Willman, K.; Kuo, K.; Murray, R. W. *J. Electroanal. Chem. Interfacial Electrochem.* **1979**, *95*, 217.
(36) Ikeda, T.; Leidner, C. R.; Murray, R. W. *J. Electroanal. Chem. Interfacial Electrochem.* **1982**, *138*, 343.
(37) Chidsey, C. E. D.; Murray, R. W. *J. Phys. Chem.* **1986**, *90*, 1479.
(38) Zaban, A.; Ferrere, S.; Gregg, B. A. *J. Phys. Chem. B* **1998**, *102*, 452.
(39) Johansson, P. G.; Kopecky, A.; Galoppini, E.; Meyer, G. J. *J. Am. Chem. Soc.* **2013**, *135*, 8331.
(40) Cappel, U. B.; Feldt, S. M.; Schöneboom, J.; Hagfeldt, A.; Boschloo, G. *J. Am. Chem. Soc.* **2010**, *132*, 9096.
(41) Lockhart, D. J.; Kim, P. S. *Science* **1992**, *257*, 947.
(42) Robson, K. C. D.; Koivisto, B. D.; Yella, A.; Sporinova, B.; Nazeeruddin, M. K.; Baumgartner, T.; Grätzel, M.; Berlinguette, C. P. *Inorg. Chem.* **2011**, *50*, 5494.
(43) Li, F.; Jennings, J. R.; Wang, Q. *ACS Nano* **2013**, *7*, 8233.
(44) Nazeeruddin, M. K.; Humphry-Baker, R.; Liska, P.; Grätzel, M. *J. Phys. Chem. B* **2003**, *107*, 8981.
(45) Chen, P.; Yum, J. H.; Angelis, F. D.; Mosconi, E.; Fantacci, S.; Moon, S.-J.; Baker, R. H.; Ko, J.; Nazeeruddin, M. K.; Grätzel, M. *Nano Lett.* **2009**, *9*, 2487.
(46) Ronca, E.; Pastore, M.; Belpassi, L.; Tarantelli, F.; De Angelis, F. *Energy Environ. Sci.* **2013**, *6*, 183.
(47) Howie, W. H.; Claeyssens, F.; Miura, H.; Peter, L. M. *J. Am. Chem. Soc.* **2008**, *130*, 1367.
(48) Rühle, S.; Greenshtein, M.; Chen, S. G.; Merson, A.; Pizem, H.; Sukenik, C. S.; Cahen, D.; Zaban, A. *J. Phys. Chem. B* **2005**, *109*, 18907.
(49) De Angelis, F.; Fantacci, S.; Selloni, A.; Grätzel, M.; Nazeeruddin, M. K. *Nano Lett.* **2007**, *7*, 3189.
(50) Heimer, T. A.; D'Arcangelis, S. T.; Farzad, F.; Stipkala, J. M.; Meyer, G. J. *Inorg. Chem.* **1996**, *35*, 5319.
(51) Bonhôte, P.; Gogniat, E.; Tingry, S.; Barbé, C.; Vlachopoulos, N.; Lenzmann, F.; Comte, P.; Grätzel, M. *J. Phys. Chem. B* **1998**, *102*, 1498.
(52) Trammell, S. A.; Meyer, T. J. *J. Phys. Chem. B* **1998**, *103*, 104.
(53) Nelson, J.; Chandler, R. E. *Coord. Chem. Rev.* **2004**, *248*, 1181.
(54) Alstrum-Acevedo, J. H.; Brennaman, M. K.; Meyer, T. J. *Inorg. Chem.* **2005**, *44*, 6802.
(55) Magnuson, A.; Anderlund, M.; Johansson, O.; Lindblad, P.; Lomoth, R.; Polivka, T.; Ott, S.; Stensjö, K.; Styring, S.; Sundström, V.; Hammarström, L. *Acc. Chem. Res.* **2009**, *42*, 1899.
(56) Song, W.; Ito, A.; Binstead, R. A.; Hanson, K.; Luo, H.; Brennaman, M. K.; Concepcion, J. J.; Meyer, T. J. *J. Am. Chem. Soc.* **2013**, *135*, 11587.
(57) Concepcion, J. J.; House, R. L.; Papanikolas, J. M.; Meyer, T. J. *Proc. Natl. Acad. Sci. U.S.A.* **2012**, *109*, 15560.